Journal of Beijing Institute of Technology, 2023, Vol. 32, No. 6

Cosserat Dynamic Modeling and Simulation of Mobile Cable on Satellite

Ziquan Wang✉, Jinzhu Li, Weinan Chen, Xuefeng Gao, You Lü, Leijie Shen, Haojie Chen

Abstract: Mainly for the problems that the configuration of the mobile cable on the satellite is very easy to change, the motion trajectory and dynamic characteristics of the cable can not be accurately predicted, which affects the laying quality seriously, the dynamic modeling and simulation of mobile cable on the satellite are carried out. On the basis of referring to the previous papers, the existing mathematical model is improved. The equations of the base vector of the cable section principal axis coordinate system with respect to the arc coordinate s, the distribution force of cable balance equation, the matrix expression of the base vector after the rotation motion transformation in the section principal axis coordinate system, the angular velocity of cable, the section elastic strain and velocity calculation equations are given, and the Cosserat dynamic modeling of the mobile cable is established. Finally, the dynamic simulation model of the mobile cable assembly of the kinematic mechanism is established, and the changes of the force and torque on the cable constraint end are obtained, which provides a reference for the dynamic modeling and simulation of the mobile cable on satellite.

Keywords: flexible cable; large deformation; curve geometry; Cosserat modeling; computer simulation

1 Introduction

The mobile cables on the satellite mainly include the mobile cables on the motion mechanism, the mobile cables during the satellite assembly process, and the mobile cables on the moving parts in the aerospace environment. Among them, the satellite motion mechanism is a component that provides motion and bearing for satellite loads such as data transmission antenna, relay antenna, synthetic aperture radar, etc. A variety of movable cables are bundled and laid on it, including power supply cables, signal cables, etc. At present, the assembly process of satellite mobile cables mainly relies on past experience to lay, bind and fix, and following the process of design, making prototype or actual physical model, motion test, improving design, preliminarily bind and fix the prototype or actual physical model of mobile cables to the accessories of mobile structures, conduct motion polarity or launch test on mobile structures, and observe the motion state of mobile cables, record the cable movement process by camera shooting or video recording. During the movement of the mechanism, if the cable has friction interference and collision with the moving mechanism, excessive bending, excessive interference torque and other phenomena, the moving cable shall be reassembled, bundled and fixed after the motion test, and the process shall be iterated step by step to ensure that the moving cable does not have friction interference and collision with the mecha-

Manuscript received Sep. 19, 2022; revised Jan. 2, 2023; accepted Apr. 4, 2023. The associate editor coordinating the review of this manuscript was Dr. Hanshu Cai. This work was supported by National Defense Basic Scientific Research Funding Project (No. JCKY2022203C048); Equipment Advanced Research Funding Program (No. 41423010401).

Ziquan Wang, Jinzhu Li, Weinan Chen, Xuefeng Gao, You Lü, Leijie Shen and Haojie Chen are with Shanghai Institute of Spacecraft Equipment, Shanghai 200240, China.

✉ Corresponding author. Email: wangziquanringse@qq.com

DOI: 10.15918/j.jbit1004-0579.2022.101

nism, and the bending radius and interference torque meet the requirements of motion. During the satellite assembly process, the mobile cables include the free moving cables during the satellite side panel enclosure process and the blind area mobile cables that cannot be observed by the operator. The laying process is still faced with difficulties such as the moving cables of the moving mechanism, especially the blind area, which are invisible and unpredictable during the assembly process, and are prone to excessive bending, resulting in the cables being physically forced to be assembled, even damaged or broken by pulling or pressing. The mobile cables on the moving parts in the aerospace environment mainly refer to that the cables installed on the satellites are forced to follow the movement because of some products, such as optical lenses, detectors, etc. In summary, it can be seen that due to the fact that mobile cables are very easy to change their configuration when laying, some cables are located in unobservable cabin sections in the blind area, the previous cable design and test interaction is frequent and the cycle is too long, and the motion trajectory and dynamic characteristics of cables during the deployment of mechanisms, satellite assembly, and component activities cannot be accurately predicted, which makes it difficult to comprehensively assess and avoid the risks after laying, and seriously affects the quality of cable laying. At present, excellent 3D CAD software such as Pro/E, CATIA, and SolidWorks are used for the cable design [1–4], but the software only carries out cable layout and configuration design based on spline curve without considering the actual physical parameters such as cable density, tensile bending stiffness, elastic modulus, shear modulus and moment of inertia, as well as the external gravity environment and distributed contact force environment in which the cable is located, The authenticity and accuracy of the cable design results are poor. Therefore, it is necessary to study the dynamic model of satellite cables, especially mobile cables, which considering physical characteristic parameters.

In terms of physical characteristics, cables can be compared to elastic slender beams. Therefore, the dynamic theory course for elastic slender beams should be applied to the dynamic modeling of cable. At present, more and more scholars at home and abroad have studied the application of elastic thin rod dynamics in engineering [5–10]. The dynamic analogy method proposed by Kirchhoff in the year of 1859 converts the deformation of the elastic rod into the rotation of the rod section along the rod centerline [11–15], so that the statics of the elastic rod has the same mathematical expression as the dynamics of the rigid body, and only the time variable t is replaced by the arc coordinate s [16–20]. After adding inertial force and time variables, it can be used for dynamic modeling of elastic rod, and has also been used in the dynamic modeling of large deformation beams in engineering [21–23]. When considering the shear and tensile deformation of the cable section, the Cosserat dynamic modeling is more suitable for the elastic thin rods. Mobile cables on the satellite have the characteristics of complex environment within the scope of activity, multiple coupling assemblies, frequent interference and collision with stars, surrounding single machines, cables and other products. Therefore, the core issue of dynamic simulation for mobile cables on the satellite is rapid dynamic simulation of assembly contact and collision.

On the basis of referring to the previous papers, this paper carries out the geometric modeling and detailed derivation of the flexible cable. According to the analysis of the curve geometric model, the equations of each dimension of the cable section principal axis coordinate system with respect to the arc coordinate s are given. Considering the distributed force elements on the center line of the actual cable physical model, the belt force balance equation is given. According to the Kardan angle transformation of the shear deformation of cable section, the matrix expres-

sion of the base vector after the centerline transformation caused by the shear deformation in the coordinate system without shear deformation is given, and the calculation equations of the cable deflection and angular velocity matrix are given. The micro arc deformation of cable is analyzed, and the calculation formulas of elastic strain and velocity of the cable section are given. Finally, the Cosserat dynamic modeling of mobile cable is carried out, which provides the theoretical basis for the motion and dynamic calculation and simulation of flexible cable.

2 The Geometry Model of Cable

2.1 The Geometry Model of Curve

The basic theory of elastic thin rod dynamic model is curve geometry. A spatial smooth curve C with length of L is shown in Fig. 1. The P_0 on the curve is the origin point, and the arc coordinate s of the curve is established under the condition that the curve has no telescopic deformation. At the same time, the fixed coordinate system O-$\xi\eta\zeta$ is established with the fixed origin point O in space, and its base vectors are $\boldsymbol{e}_\xi$, $\boldsymbol{e}_\eta$, $\boldsymbol{e}_\zeta$. Then the arbitrary point P on the curve can be determined by the arc coordinate s and the vector diameter $\boldsymbol{r}$ relative to the fixed point O. $\boldsymbol{r}$ is the vector that completely determines the geometry of curve C and the single value continuous differentiable function about the arc coordinate s. Then the tangent direction unit vector of curve C at point P is

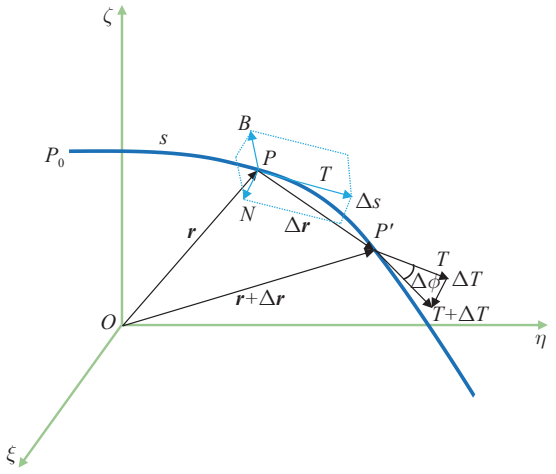

Fig. 1 Infinitesimal angular displacement and the Frenet coordinates of spatial smooth curve

$$T(s)=\frac{\mathrm{d}r}{\mathrm{d}s} \tag{1}$$

The modulus of derivative of the $\boldsymbol{T}(s)$ on s is defined as the curvature of curve C at point P, and the expression is

$$\kappa=\left|\frac{\mathrm{d}T}{\mathrm{d}s}\right| \tag{2}$$

Define the infinitesimal angular displacement when point P on curve C moving to the adjacent point P' as $\Delta\phi$. When $\Delta s\to 0$, the curvature expression is

$$\kappa=\lim_{\Delta s\to 0}\frac{\Delta\phi}{\Delta s}=\frac{\mathrm{d}\phi}{\mathrm{d}s} \tag{3}$$

Therefore, curvature is a parameter to measure the degree of curve bending, and its reciprocal is called the radius of curvature

$$\rho(s)=\frac{1}{\kappa} \tag{4}$$

The unit vector along the direction $\mathrm{d}\boldsymbol{T}/\mathrm{d}s$ is called the normal vector of curve C at point P, which is recorded as

$$\boldsymbol{N}(s)=\frac{\mathrm{d}\boldsymbol{T}}{\kappa\mathrm{d}s} \tag{5}$$

According to the right-hand spiral rule of the coordinate system, the sub-normal vector of curve C at point P is recorded as

$$\boldsymbol{B}(s)=\boldsymbol{T}(s)\times\boldsymbol{N}(s) \tag{6}$$

In Fig. 1, the coordinate system composed of P-$\boldsymbol{NBT}$ is the Frenet coordinate system, and its base vectors $\boldsymbol{e}_n$, $\boldsymbol{e}_b$, $\boldsymbol{e}_t$ are equal to $\boldsymbol{N}$, $\boldsymbol{B}$, $\boldsymbol{T}$. The plane formed by $\boldsymbol{T}$ and $\boldsymbol{N}$ is the osculating plane, and the plane formed by $\boldsymbol{N}$ and $\boldsymbol{B}$ is the normal plane. Suppose point P moves in the positive direction of arc coordinate s at unit speed along curve C, then the rotation angular velocity of the normal plane around axis $\boldsymbol{B}$ is $\kappa(s)$, and the rotation angular velocity vector of the osculating plane around axis $\boldsymbol{T}$ is

$$\boldsymbol{\tau} = \frac{\mathrm{d}\boldsymbol{B}}{\mathrm{d}s} \tag{7}$$

The modulus of $\boldsymbol{\tau}(s)$ is called the torsion of curve C at point P, so the rotational angular velocity of the Frenet coordinate system relative to the fixed coordinate system O-$\xi\eta\zeta$ is

$$\boldsymbol{\omega}_F(s) = \kappa\boldsymbol{B} + \tau\boldsymbol{T} \tag{8}$$

According to Eq. (1) to Eq. (8), the equations of each dimension of Frenet coordinate system with respect to the arc coordinate s can be obtained

$$\frac{\mathrm{d}\boldsymbol{N}}{\mathrm{d}s} = \tau\boldsymbol{B} - \kappa T,\ \frac{\mathrm{d}\boldsymbol{B}}{\mathrm{d}s} = -\tau N,\ \frac{\mathrm{d}\boldsymbol{T}}{\mathrm{d}s} = \kappa\boldsymbol{N} \tag{9}$$

Then the position of the space curve C relative to the fixed coordinate system can be obtained from the following equation as

$$r(s) = \int_0^s T(\sigma)\mathrm{d}(\sigma) + r(0) \tag{10}$$

In Eq. (10), σ is the integral variable, and $\boldsymbol{r}(0)$ represents the spatial position of point P_0. According to Eq. (8) to Eq. (10), curvature and torsion are two independent variables to determine the spatial curve. Therefore, it can be seen that the freedom degree of the spatial curve is 2.

2.2 The Geometric Bending and Torsion of Cable

As shown in Fig. 2, the section principal axis coordinate system P-xyz rotates a torsion angle around the axis of $\boldsymbol{T}$ relative to the Frenet coordinate system. The base vectors of the section principal axis coordinate system P-xyz are $\boldsymbol{e}_1$, $\boldsymbol{e}_2$, $\boldsymbol{e}_3$. It can be obtained that the angular velocity vector of the cable section relative to the fixed coordinate system O-$\xi\eta\zeta$ is

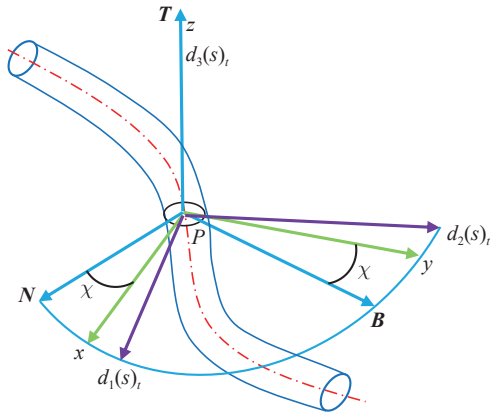

Fig. 2 The Frenet coordinate system and the principal axis coordinate system of the cable section

$$\begin{cases} \boldsymbol{\omega} = \omega_1\boldsymbol{e}_1 + \omega_2\boldsymbol{e}_2 + \omega_3\boldsymbol{e}_3 \\ \omega_1 = \kappa\sin\chi, \omega_2 = \kappa\cos\chi, \omega_3 = \tau + \dfrac{\mathrm{d}\chi}{\mathrm{d}s} \end{cases} \tag{11}$$

It is knowable that $\boldsymbol{\omega}$ is the vector of cable bending and torsional deformation, which is called bending and torsion degree, and the three components of bending and torsion degree $\boldsymbol{\omega}_i$(i=1, 2, 3) are the three independent variables that determine the geometric form. Similarly, other coordinate systems P-$d_1(s)_t d_2(s)_t d_3(s)_t$ whose origin is the point P can also be associated with coordinate rotation.

From the coordinate change relationship, the equations of each dimension of P-xyz coordinate system with respect to arc coordinate s can be obtained

$$\begin{cases} \dfrac{\mathrm{d}\boldsymbol{e}_1}{\mathrm{d}s} = \left(\tau + \dfrac{\mathrm{d}\chi}{\mathrm{d}s}\right)\boldsymbol{e}_2 - \kappa\cos\chi\boldsymbol{e}_3 \\ \dfrac{\mathrm{d}\boldsymbol{e}_2}{\mathrm{d}s} = -\left(\tau + \dfrac{\mathrm{d}\chi}{\mathrm{d}s}\right)\boldsymbol{e}_1 + \kappa\sin\chi\boldsymbol{e}_3 \\ \dfrac{\mathrm{d}\boldsymbol{e}_3}{\mathrm{d}s} = \kappa(\cos\chi\boldsymbol{e}_1 - \sin\chi\boldsymbol{e}_2) \end{cases} \tag{12}$$

3 Distribution Force Balance Equation of Cable

Considering the possible contact or mutual contact between cables and other objects, there must be a distributed contact force. If the electrostatic effect between cables is considered, the distributed electrostatic attraction must be introduced. When discussing the movement of cables in viscous medium, the viscous resistance and moment must also be introduced. Therefore, the balance equation should take the distributed force and moment into account.

As shown in Fig. 3, the force balance diagram of $P - P'$ micro arc section under distributed force, gravity and gravity moment. In the figure, $\boldsymbol{M}$ is the moment, $\boldsymbol{F}$ is the force, $\boldsymbol{f}$ and $\boldsymbol{m}$ are the distributed force and moment, $\boldsymbol{f}_g$

and $\boldsymbol{m}_{\mathrm{g}}$ are the gravity, and gravity moment, respectively. It can be seen that the resultant force and resultant moment at point P are zero in the equilibrium state, that is

$$\begin{cases} \Delta \boldsymbol{F} + \boldsymbol{f}\Delta s + \boldsymbol{f}_{\mathrm{g}}\Delta s = 0 \\ \Delta \boldsymbol{M} + \Delta \boldsymbol{r} \times \boldsymbol{F} + \boldsymbol{m}\Delta s + \boldsymbol{m}_{\mathrm{g}}\Delta s = 0 \end{cases} \tag{13}$$

Divide Eq. (13) by Δs and let $\Delta s \to 0$, and simultaneous Eq. (1) we can get

$$\begin{cases} \dfrac{\mathrm{d}\boldsymbol{F}}{\mathrm{d}s} + \boldsymbol{f} + \boldsymbol{f}_g = 0 \\ \dfrac{\mathrm{d}\boldsymbol{M}}{\mathrm{d}s} + \boldsymbol{T} \times \boldsymbol{F} + \boldsymbol{m} + \boldsymbol{m}_g = 0 \end{cases} \tag{14}$$

Convert Eq. (14) to *P*-*xyz* coordinate system, we can obtain

$$\begin{cases} \dfrac{\mathrm{d}\boldsymbol{F}}{\mathrm{d}s} + \boldsymbol{\omega} \times \boldsymbol{F} + \boldsymbol{f} + \boldsymbol{f}_{\mathrm{g}} = 0 \\ \dfrac{\mathrm{d}\boldsymbol{M}}{\mathrm{d}s} + \boldsymbol{\omega} \times \boldsymbol{M} + \boldsymbol{e}_3 \times \boldsymbol{F} + \boldsymbol{m} + \boldsymbol{m}_{\mathrm{g}} = 0 \end{cases} \tag{15}$$

Then the projection of the resultant force and resultant moment on *P*-*xyz* coordinate system is

$$\begin{cases} \dfrac{\mathrm{d}F_1}{\mathrm{d}s} + \kappa \cos\chi F_3 - \left(\tau + \dfrac{\mathrm{d}\chi}{\mathrm{d}s}\right) F_2 + f_1 + f_{\mathrm{g}1} = 0 \\ \dfrac{\mathrm{d}F_2}{\mathrm{d}s} + \left(\tau + \dfrac{\mathrm{d}\chi}{\mathrm{d}s}\right) F_1 - \kappa \sin\chi F_3 + f_2 + f_{\mathrm{g}2} = 0 \\ \dfrac{\mathrm{d}F_3}{\mathrm{d}s} + \kappa \sin\chi F_2 - \kappa \cos\chi F_1 + f_3 + f_{\mathrm{g}3} = 0 \\ \dfrac{\mathrm{d}M_1}{\mathrm{d}s} + \kappa \cos\chi M_3 - \left(\tau + \dfrac{\mathrm{d}\chi}{\mathrm{d}s}\right) M_2 - F_2 + \\ \quad m_1 + m_{\mathrm{g}1} = 0 \\ \dfrac{\mathrm{d}M_2}{\mathrm{d}s} + \left(\tau + \dfrac{\mathrm{d}\chi}{\mathrm{d}s}\right) M_1 - \kappa \sin\chi M_3 + F_1 + \\ \quad m_2 + m_{\mathrm{g}2} = 0 \\ \dfrac{\mathrm{d}M_3}{\mathrm{d}s} + \kappa \sin\chi M_2 - \kappa \cos\chi M_1 + m_3 + m_{\mathrm{g}3} = 0 \end{cases} \tag{16}$$

It should be pointed out that if the friction or tangential gravity is not considered, the force f_3=0. If the distributed forces are omitted, the equation will become the equilibrium equations without scoring the distributed forces. The distributed moment appears only when moving in a viscous medium, so it can be omitted in the discussion of statics.

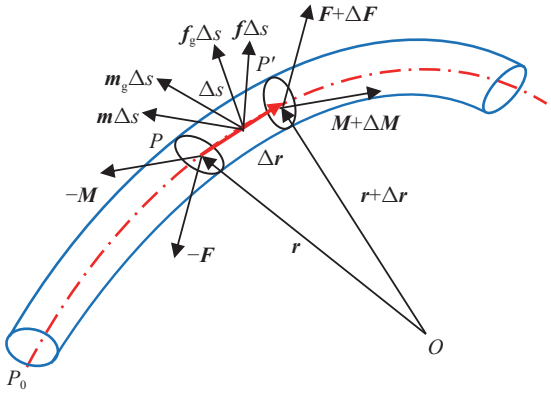

Fig. 3 Distributed force balance of cable micro arc section

Since the cables on the satellite are in the power-off state when laying or moving, the electrostatic attraction between cables can be ignored. The viscosity coefficient of air is very small, so the viscous resistance of the cable moving in the air can also be ignored. However, due to the existence of earth gravity and cable indirect contact force, the distributed force on the cable can not be ignored.

4 Dynamic Model of Cable

4.1 Angle Transformation of Kardan with Shear Deformation

Before making the Kardan angle transformation, it is necessary to point out the section deformation as follows.

1) Geometric characteristics: The cable has certain quality and deformability; Compared with the cross-sectional size, the cable is much larger in length and radius of curvature; Due to the bending and torsion of the cable itself, the two sections of the same cable micro section can rotate relative to the center line.

2) Physical properties: Take the cable with circular section, the material is homogeneous and isotropic, and the stress and strain meet the linear constitutive relationship; The cross section of the cable end is regarded as a rigid plane that cannot be deformed.

As shown in Fig. 4, the cable section attitude is described using the Kardan angle coordinate transformation system. The Kardan angle

transformation needs to consider four groups of coordinate systems: O-$\xi\eta\zeta$ (fixed coordinate system), P-xyz (section principal axis coordinate system), P-$x_0y_0z_0$ (transition coordinate system) and P-$x_sy_sz_s$ (section normal and section fixed coordinate system). Moving the origin O of the coordinate system to the point P on the cable in the figure, ψ is the rotation angle around the ξ axis from the coordinate system P-$x_0y_0z_0$; θ is the rotation angle of P-$x_0y_0z_0$ around the axis y_0 to the coordinate system P-xyz, where the z-axis is the normal axis of the section; φ refers to the rotation angle of P-xyz around the z-axis, to the coordinate system P-$x_sy_sz_s$, and fixed with the section, the Kardan angle ψ, θ, φ determine the attitude of the section after rotation.

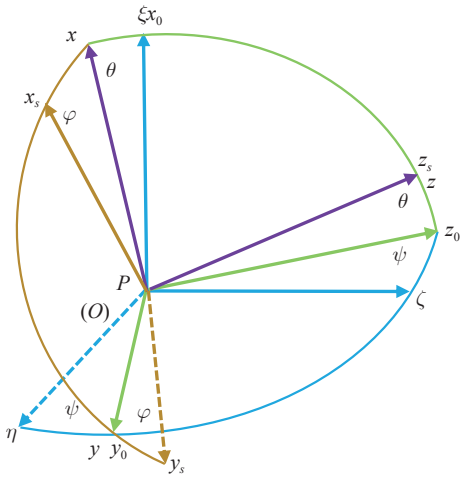

Fig. 4 Angle transformation of Kardan

Take $\boldsymbol{e}_3$ as the base vector, the section has no strain in the O-xy plane, and an infinitesimal rotation vector $\boldsymbol{\delta}$ is generated in the center of the section in the O-xz and O-yz planes to the coordinate system P-$x^*y^*z^*$, where the z^*-axis direction is along the tangent direction of the centerline, as shown in Fig. 5. Note that the strain in the P-xyz coordinate system is $\varepsilon_1 = \delta_{13}, \varepsilon_2 = -\delta_{23}$, then the projection of $\boldsymbol{\delta}$ in the P-xyz coordinate system is

$$\boldsymbol{\delta} = [\delta_{23} \quad \delta_{13} \quad 0]^{\mathrm{T}} = [-\varepsilon_2 \quad \varepsilon_1 \quad 0]^{\mathrm{T}} \tag{17}$$

The z^*-axis of the coordinate system P-$x^*y^*z^*$ is the position after the rotation of the z-axis of P-xyz. The base vector $\boldsymbol{e}^*$ is expressed in P-xyz. Taylor expansion is carried out for small variables δ_{13}, δ_{23}, and the quadratic small quantity is ignored. The expression of the base vector $\boldsymbol{e}^*$ in P-xyz is as follows

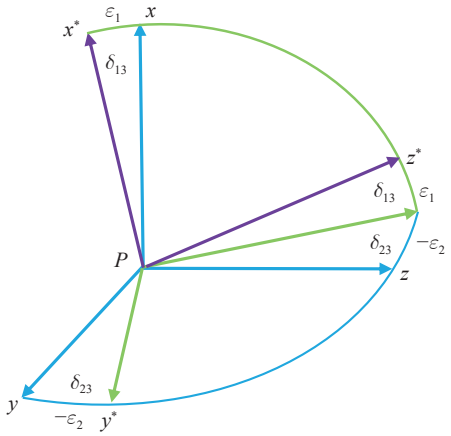

Fig. 5 Centerline rotation transformation

$$\boldsymbol{e}^* = \begin{bmatrix} \boldsymbol{e}_1^* & \boldsymbol{e}_2^* & \boldsymbol{e}_3^* \end{bmatrix} = \begin{bmatrix} 1 & 0 & \varepsilon_1 \\ -\varepsilon_1\varepsilon_2 & 1 & \varepsilon_2 \\ -\varepsilon_1 & -\varepsilon_2 & 1 \end{bmatrix} \tag{18}$$

Eq. (18) is the matrix expression of the base vector transformed by the centerline caused by shear deformation in the coordinate system without shear deformation.

Let the matrix $\boldsymbol{A}$ be the rotation matrix of the rigid body around the local rectangular coordinate system. According to the rotation kinematics of the coordinate system, we can get

$$\begin{cases} \boldsymbol{A}_{x,\psi} = \begin{bmatrix} 1 & 0 & 0 \\ 0 & \cos\psi & \sin\psi \\ 0 & -\sin\psi & \cos\psi \end{bmatrix} \\ \boldsymbol{A}_{y,\theta} = \begin{bmatrix} \cos\theta & 0 & -\sin\theta \\ 0 & 1 & 0 \\ \sin\theta & 0 & \cos\theta \end{bmatrix} \\ \boldsymbol{A}_{z,\varphi} = \begin{bmatrix} \cos\varphi & \sin\varphi & 0 \\ -\sin\varphi & \cos\varphi & 0 \\ 0 & 0 & 1 \end{bmatrix} \end{cases} \tag{19}$$

Let the transient rate of change of the angular displacement of P-xyz to the arc coordinate s and time t be recorded as $\boldsymbol{\omega}$ and $\boldsymbol{\Omega}$, the transient change rate of the angular displacement of P-$x_sy_sz_s$ to the arc coordinate s and time t is recorded as $\boldsymbol{\omega}_s$ and $\boldsymbol{\Omega}_s$, note that ω' is the derivative of angular displacement to arc coordinate s and $\dot{\Omega}$ is the derivative of angular displacement

at time t. The expression of the transient change rate of angular displacement of P-$x_s y_s z_s$ to the arc coordinate s in O-$\xi\eta\zeta$ is

$$
\begin{aligned}
{}_O\boldsymbol{\omega}_s =& \boldsymbol{\omega}_{s1O}\boldsymbol{e}_1 + \boldsymbol{\omega}_{s2O}\boldsymbol{e}_2 + \boldsymbol{\omega}_{s3O}\boldsymbol{e}_3 = \\
& \psi'_O\boldsymbol{e}_1 + \theta'_O\boldsymbol{e}_2 + \varphi'_s\boldsymbol{e}_3 = \\
& \begin{bmatrix} \cos\theta\cos\varphi & \sin\varphi & 0 \\ -\cos\theta\sin\varphi & \cos\varphi & 0 \\ \sin\theta & 0 & 1 \end{bmatrix} \begin{bmatrix} \psi' \\ \theta' \\ \varphi' \end{bmatrix}
\end{aligned} \tag{20}
$$

The expression of the transient change rate of the angular displacement of P-xyz to the arc coordinate s in O-$\xi\eta\zeta$ is

$$
\begin{aligned}
{}_O\boldsymbol{\omega} =& \boldsymbol{\omega}_{1O}\boldsymbol{e}_1 + \boldsymbol{\omega}_{2O}\boldsymbol{e}_2 + \boldsymbol{\omega}_{3O}\boldsymbol{e}_3 = \\
& \psi'_O\boldsymbol{e}_1 + \theta'_O\boldsymbol{e}_2 + 0\cdot\varphi'\boldsymbol{e}_3 = \\
& \begin{bmatrix} \cos\theta\cos\varphi & \sin\varphi & 0 \\ -\cos\theta\sin\varphi & \cos\varphi & 0 \\ \sin\theta & 0 & 0 \end{bmatrix} \begin{bmatrix} \psi' \\ \theta' \\ \varphi' \end{bmatrix}
\end{aligned} \tag{21}
$$

It can be seen from Eq. (20) and (21) that the transient change rate of the angular displacement of P-xyz to the arc coordinate s is equal to the transient change rate of the angular displacement of P-$x_s y_s z_s$ to the arc coordinate s in the $[\psi'\ \theta']$ dimension. Then the matrix calculation equation of the transient change rate of the angular displacement of P-$x_s y_s z_s$ and P-xyz to the arc coordinate s in P-xyz is

$$
\begin{cases}
\boldsymbol{\omega}_s = \boldsymbol{A}_{y,\theta}\boldsymbol{A}_{x,\varphi}[\boldsymbol{A}_{z,\varphi}\boldsymbol{A}_{y,\theta}\boldsymbol{A}_{x,\varphi}]^{-1}{}_O\boldsymbol{\omega}_s \\
\boldsymbol{\omega} = A_{y,\theta}\boldsymbol{A}_{x,\varphi}[\boldsymbol{A}_{z,\varphi}\boldsymbol{A}_{y,\theta}\boldsymbol{A}_{x,\varphi}]^{-1}{}_O\boldsymbol{\omega}
\end{cases} \tag{22}
$$

From Eq. (19) to Eq. (22), we can get

$$
\begin{aligned}
\boldsymbol{\omega}_s =& [\ \omega_{s1}\quad \omega_{s2}\quad \omega_{s3}\ ]^{\mathrm{T}} = \\
& [\ \psi'\cos\theta\quad \theta'\quad \psi'\sin\theta\ +\varphi']^{\mathrm{T}}
\end{aligned} \tag{23}
$$

$$
\begin{aligned}
\boldsymbol{\omega} =& [\ \omega_1\quad \omega_2\quad \omega_3\ ]^{\mathrm{T}} = \\
& [\ \psi'\cos\theta\quad \theta'\quad \psi'\sin\theta\ ]^{\mathrm{T}}
\end{aligned} \tag{24}
$$

Similarly, it can be obtained that the transient change rate of angular displacement of P-$x_s y_s z_s$ and P-xyz at time t is expressed in P-xyz as

$$
\begin{aligned}
\boldsymbol{\Omega}_s =& [\ \Omega_{s1}\quad \Omega_{s2}\quad \Omega_{s3}\ ]^{\mathrm{T}} = \\
& [\ \dot{\psi}\cos\theta\quad \dot{\theta}\quad \dot{\psi}\sin\theta\ +\dot{\varphi}]^{\mathrm{T}}
\end{aligned} \tag{25}
$$

$$
\begin{aligned}
\boldsymbol{\Omega} =& [\ \Omega_1\quad \Omega_2\quad \Omega_3\ ]^{\mathrm{T}} = \\
& [\ \dot{\psi}\cos\theta\quad \dot{\theta}\quad \dot{\psi}\sin\theta\ ]^{\mathrm{T}}
\end{aligned} \tag{26}
$$

The principle of micro-arc deformation of cable which is shown in Fig. 6. In order to understand the deformation principle of the cable micro arc segment, the basic vector $\boldsymbol{e}_3$ of the section principal axis coordinate system and the z-direction elastic strain are added to the micro arc segment deformation body ε_3, the cable section shows tensile deformation when moving along the z-axis; when rotating around the z-axis, it shows torsional deformation. When moving along the axis of x or y, it shows shear deformation. When rotating around the axis of x or y, it shows the bending deformation.

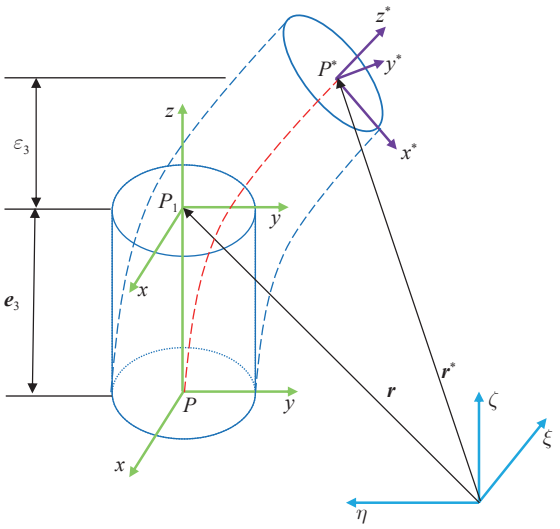

Fig. 6 Micro arc deformation and strain along z-direction

Before the elastic deformation of the cable, take the micro arc segment Δs and $\boldsymbol{r}(s,t)$ along the center line of point P as the vector diameter of point P relative to the fixed point O, we can get

$$
\Delta\boldsymbol{r} = \Delta s\boldsymbol{e}_3 \tag{27}
$$

Then the partial derivative of vector diameter $\boldsymbol{r}$ on s is

$$
\frac{\partial\boldsymbol{r}}{\partial s} = \boldsymbol{r}' = \lim_{\Delta s\to 0}\frac{\Delta\boldsymbol{r}}{\Delta s} = \boldsymbol{e}_3 \tag{28}
$$

Consider the vector diameter after deformation $\boldsymbol{r}^*(s,t)$, and set ε_1, ε_2, ε_3 are the projection of the deformed strain on P-xyz, we can get

$$
\Delta\boldsymbol{r}^* = \Delta s(1+\varepsilon_3)\boldsymbol{e}_3^* \tag{29}
$$

From Eq. (27) to Eq. (29), it can be obtained

$$\begin{cases} \dfrac{\partial \boldsymbol{r}^*}{\partial s} = \lim\limits_{\Delta s \to 0} \dfrac{\Delta \boldsymbol{r}^*}{\Delta s} = (1+\varepsilon_3)\boldsymbol{e}_3^* = \boldsymbol{\varepsilon} + \boldsymbol{e}_3 \\ \boldsymbol{\varepsilon} = [\ \varepsilon_1 \quad \varepsilon_2 \quad \varepsilon_3\ ] \end{cases} \tag{30}$$

The representation of the component of the vector diameter $\boldsymbol{r}^*$ in the fixed coordinate is recorded as $\xi(s), \eta(s), \zeta(s)$, the representation of the vector diameter $\boldsymbol{r}_{(0)}$ in the fixed coordinate is recorded as $\xi_0(s), \eta_0(s), \zeta_0(s)$, and the displacement due to the shear deformation and expansion deformation of the body of the section is recorded as $\boldsymbol{w}(s,t)$, then we get

$$\begin{cases} \boldsymbol{w}(s,t) = \boldsymbol{r}^*(s,t) - \boldsymbol{r}_{(0)}(s) \\ \boldsymbol{r}_{(0)}(s) = \xi_0(s)\boldsymbol{e}_\xi + \eta_0(s)\boldsymbol{e}_\eta + \zeta_0(s)\boldsymbol{e}_\zeta \end{cases} \tag{31}$$

The derivation of the arc coordinate s in Eq. (31) in the coordinate system *P-xyz* is expressed as

$$\begin{aligned} \frac{\partial \boldsymbol{w}}{\partial s} &= \frac{\tilde{\partial}\boldsymbol{w}}{\partial s} + \boldsymbol{\omega} \times \boldsymbol{w} = \frac{\tilde{\partial}}{\partial s}\left[\boldsymbol{r}^*(s,t) - \boldsymbol{r}_{(0)}(s)\right] \\ &= \boldsymbol{e}_3 + \boldsymbol{\varepsilon} - \boldsymbol{e}_{3(0)} \end{aligned} \tag{32}$$

In Eq. (32), the $e_{3(0)}$ can be determined by the initial Kardan angle ψ_0, θ_0, after rotation transformation, it can be obtained

$$\begin{aligned} &{}_O\boldsymbol{e}_{(0)} = [\ {}_O\boldsymbol{e}_{1(0)} \quad {}_O\boldsymbol{e}_{2(0)} \quad {}_O\boldsymbol{e}_{3(0)}\ ]^{\mathrm{T}} = \\ &\boldsymbol{A}_{y,\theta_{(0)}}\boldsymbol{A}_{x,\psi_{(0)}}[\ \boldsymbol{e}_\xi \quad \boldsymbol{e}_\eta \quad \boldsymbol{e}_\zeta\ ]^{\mathrm{T}} = \\ &\begin{bmatrix} \cos\theta_{(0)} & \sin\psi_{(0)}\sin\theta_{(0)} & -\cos\psi_{(0)}\sin\theta_{(0)} \\ 0 & \cos\psi_{(0)} & \sin\psi_{(0)} \\ \sin\theta_{(0)} & -\sin\psi_{(0)}\cos\theta_{(0)} & \cos\psi_{(0)}\cos\theta_{(0)} \end{bmatrix} \begin{bmatrix} \boldsymbol{e}_\xi \\ \boldsymbol{e}_\eta \\ \boldsymbol{e}_\zeta \end{bmatrix} \end{aligned} \tag{33}$$

Therefore

$${}_O\boldsymbol{e}_{3(0)} = \sin\theta_{(0)}\boldsymbol{e}_\xi - \sin\psi_0\cos\theta_{(0)}\boldsymbol{e}_\eta + \cos\psi_0\cos\theta_0\boldsymbol{e}_\zeta \tag{34}$$

If Eq. (34) is expressed in *P-xyz* coordinate system, it can be obtained

$$\begin{aligned} &\boldsymbol{e}_{3(0)} = \boldsymbol{A}_{y,\theta}\boldsymbol{A}_{x,\psi O}\boldsymbol{e}_{3(0)}[\ \boldsymbol{e}_1 \quad \boldsymbol{e}_2 \quad \boldsymbol{e}_3\ ]^{\mathrm{T}} = \\ &\begin{pmatrix} [\sin\theta_0\cos\theta - \cos\theta_0\sin\theta\cos(\psi-\psi_0)]\,\boldsymbol{e}_1 \\ [\cos\theta_0\sin(\psi-\psi_0)]\,\boldsymbol{e}_2 \\ [\sin\theta_0\sin\theta + \cos\theta_0\cos\theta\cos(\psi-\psi_0)]\,\boldsymbol{e}_3 \end{pmatrix} \end{aligned} \tag{35}$$

According to Eq. (24) and Eq. (32), we can get

$$\frac{\tilde{\partial}\boldsymbol{w}}{\partial s} = \begin{bmatrix} \dfrac{\partial w_1}{\partial s} & \dfrac{\partial w_2}{\partial s} & \dfrac{\partial w_3}{\partial s} \end{bmatrix}^{\mathrm{T}} = [\ w_1' \quad w_2' \quad w_3'\ ]^{\mathrm{T}} \tag{36}$$

$$\boldsymbol{\omega} \times \boldsymbol{w} = \begin{bmatrix} w_3\theta' - w_2\psi'\sin\theta \\ \psi'(w_1\sin\theta - w_3\cos\theta) \\ w_2\psi'\cos\theta - w_1\theta' \end{bmatrix} \tag{37}$$

According to Eq. (32), simultaneous Eq. (33) to Eq. (37), we can get

$$\begin{aligned} \boldsymbol{\varepsilon} = [\ \varepsilon_1 \quad \varepsilon_2 \quad \varepsilon_3\ ]^{\mathrm{T}} = \frac{\tilde{\partial}\boldsymbol{w}}{\partial s} + \boldsymbol{\omega}\times\boldsymbol{w} - \boldsymbol{e}_3 + \boldsymbol{e}_{3(0)} = \\ \begin{bmatrix} w_1' + w_3\theta' - w_2\psi'\sin\theta + \\ \ \sin\theta_0\cos\theta - \cos\theta_0\sin\theta\cos(\psi-\psi_0) \\ w_2' + \psi'(w_1\sin\theta - w_3\cos\theta) + \\ \ \cos\theta_0\sin(\psi-\psi_0) \\ w_3' + w_2\psi'\cos\theta - w_1\theta' - 1 + \\ \ \sin\theta_0\sin\theta + \cos\theta_0\cos\theta\cos(\psi-\psi_0) \end{bmatrix} \end{aligned} \tag{38}$$

The Eq. (38) is the strain matrix after considering shear and tensile deformation. It can be seen that the strain matrix of the cable section is related to the displacement $\boldsymbol{w}$, Kardan angle $\psi, \theta$and initial Kardan angle $\psi_{(0)}, \theta_{(0)}$ caused by telescopic deformation. Convert the arc coordinate s into time t according to Eq. (26), Eq. (32), and Eq. (38), the expression of the speed of the cable section in the *P-xyz* coordinate system is expressed as

$$\begin{aligned} \boldsymbol{v} = \frac{\partial \boldsymbol{r}^*}{\partial t} = \frac{\tilde{\partial}\boldsymbol{w}}{\partial t} + \boldsymbol{\Omega}\times\boldsymbol{w} = [\ v_1 \quad v_2 \quad v_3\ ]^{\mathrm{T}} = \\ \begin{bmatrix} \dot{w}_1 + w_3\dot{\theta} - w_2\dot{\psi}\sin\theta \\ \dot{w}_2 + \dot{\psi}(w_1\sin\theta - w_3\cos\theta) \\ \dot{w}_3 + w_2\dot{\psi}\cos\theta - w_1\dot{\theta} \end{bmatrix} \end{aligned} \tag{39}$$

It can be seen that ψ, θ, φ, w_1, w_2, w_3 are the six generalized coordinates to determine the cable configuration, and the bending torsion, the section angular velocity, elastic strain, and velocity parameters of the rod can be determined by the derivatives of these six generalized coordinates to the arc coordinate s and time t.

4.2 Dynamic Model of Cable

Define the cable shear stiffness coefficient as K; The tensile stiffness coefficient is K_0; the bending

stiffness of the section around the x-axis is $A(A=EI_x)$, E is the elastic modulus, and I_x is the moment of inertia of the section relative to the x-axis; the bending stiffness of the section around the y-axis is $B(B=EI_y)$, and I_y is the moment of inertia of the section relative to the y-axis; The torsional stiffness of the section around the z-axis is $C(C=GI_z)$, G is the cable shear modulus, and I_z is the polar moment of inertia of the section relative to the z-axis; ρ is the density of the cable; S is the cross-sectional area of the cable; $\boldsymbol{J}$ is the inertia tensor of per unit length of cable; The bending and torsion of the cable in the initial state is

$$\boldsymbol{\omega}_{s0} = \begin{bmatrix} \omega_{s1}^0 & \omega_{s2}^0 & \omega_{s3}^0 \end{bmatrix}^{\mathrm{T}} \tag{40}$$

Then the projection of forces and moments on the coordinate system P-xyz is

$$\begin{cases} F_1 = K\varepsilon_1 \\ F_2 = K\varepsilon_2 \\ F_3 = K_0\varepsilon_3 \\ M_1 = A(\omega_{s1} - \omega_{s1}^0) \\ M_2 = B(\omega_{s2} - \omega_{s3}^0) \\ M_3 = C(\omega_{s3} - \omega_{s3}^0) \end{cases} \tag{41}$$

According to the momentum theorem and momentum moment theorem of Newtonian mechanics, the cable dynamics model can be obtained as follows

$$\begin{cases} \boldsymbol{F}' + \boldsymbol{\omega} \times \boldsymbol{F} + \boldsymbol{f} + \boldsymbol{f}_{\mathrm{g}} - \rho S(\dfrac{\partial v}{\partial t} + \boldsymbol{\Omega} \times \boldsymbol{v}) = 0 \\ \boldsymbol{M}' + \boldsymbol{\omega} \times \boldsymbol{M} + \boldsymbol{m} + \boldsymbol{m}_{\mathrm{g}} + (\boldsymbol{e}_3 + \boldsymbol{\varepsilon}) \times \boldsymbol{F} - \\ \dfrac{\partial(\boldsymbol{J} \cdot \boldsymbol{\Omega}_s)}{\partial \boldsymbol{t}} - \boldsymbol{\Omega} \times (\boldsymbol{J} \cdot \boldsymbol{\Omega}_s) = 0 \end{cases} \tag{42}$$

Let the moment of inertia of J along the axes of x and y be ρI. Then the moment of inertia along the z-axis is $2\rho I$. Set J_0 and I as the moment of inertia of the section. Consider the cable with circular section, we can get

$$\begin{cases} \boldsymbol{J} = \mathrm{diag}(\ J \quad J \quad J_0\ ) \\ J_0 = 2J \\ A = B \end{cases} \tag{43}$$

Thus

$$\boldsymbol{J} \cdot \boldsymbol{\Omega}_s = \begin{bmatrix} J\dot{\psi}\cos\theta \\ J\dot{\theta} \\ \dot{\psi}\sin\theta + \dot{\varphi} \end{bmatrix} \tag{44}$$

Order that

$$\begin{cases} \dfrac{\partial \gamma}{\partial s} = \dfrac{\partial \psi}{\partial s}\sin\theta + \dfrac{\partial \varphi}{\partial s} \\ \dfrac{\partial \gamma}{\partial t} = \dfrac{\partial \psi}{\partial t}\sin\theta + \dfrac{\partial \varphi}{\partial t} \end{cases} \tag{45}$$

Then we get

$$\boldsymbol{J} \cdot \boldsymbol{\Omega}_s = \begin{bmatrix} J\dot{\psi}\cos\theta & J\dot{\theta} & \dot{\gamma} \end{bmatrix}^{\mathrm{T}} \tag{46}$$

$$\frac{\partial \boldsymbol{J} \cdot \boldsymbol{\Omega}_s}{\partial t} = \begin{bmatrix} J\ddot{\psi}\cos\theta - J\dot{\psi}\dot{\theta}\sin\theta & J\ddot{\theta} & \ddot{\gamma} \end{bmatrix}^{\mathrm{T}} \tag{47}$$

The Cosserat dynamic model of the circular section cable can be obtained by simultaneous Eq. (41) to Eq. (47)

$$\begin{cases} F_1' + F_3\theta' - F_2\psi'\sin\theta + f_1 + f_{\mathrm{g}1} - \\ \quad \rho S(\dot{v}_1 + v_3\dot{\theta} - v_2\dot{\psi}\sin\theta) = 0 \\ F_2' + \psi'(F_1\sin\theta - F_3\cos\theta) + f_2 + f_{\mathrm{g}2} \\ \quad -\rho S[\dot{v}_2 + \dot{\psi}(v_1\sin\theta - v_3\cos\theta)] = 0 \\ F_3' + F_2\psi'\cos\theta - F_1\theta' + f_3 + f_{\mathrm{g}3} - \\ \quad \rho S(\dot{v}_3 + v_2\dot{\psi}\cos\theta - v_1\dot{\theta}) = 0 \\ A[\psi''\cos\theta - \omega_{s1'}^0 - \psi'\sin\theta(2\theta' - \omega_{s2}^0)] \\ \quad + C\theta'(\gamma' - \omega_{s3}^0) - (1+\varepsilon_3)F_2 + \varepsilon_2 F_3 - \\ \quad J(\ddot{\psi}\cos\theta - 2\dot{\psi}\dot{\theta}\sin\theta) - J_0\dot{\gamma}\dot{\theta} + \\ \quad m_1 + m_{\mathrm{g}1} = 0 \\ B[\theta'' - \omega_{s2'}^0 + \psi'\sin\theta(\psi'\cos\theta - \omega_{s1}^0)] - \\ \quad C\psi'\cos\theta(\gamma' - \omega_{s3}^0) + (1+\varepsilon_3)F_1 - \varepsilon_1 F_3 \\ \quad -J[\ddot{\theta} + \dot{\psi}^2\sin\theta\cos\theta] + J_0\dot{\gamma}\dot{\psi}\cos\theta + \\ \quad m_2 + m_{\mathrm{g}2} = 0 \\ C(\gamma'' - \omega_{s3'}^0) + A(\omega_{s1}^0\theta' - \omega_{s2}^0\psi'\cos\theta) - \\ \quad J_0\ddot{\gamma} - F_1\varepsilon_2 + F_2\varepsilon_1 + \\ \quad m_3 + m_{\mathrm{g}3} = 0 \end{cases} \tag{48}$$

The Eq. (48) is the Cosserat dynamic model mobile cable. Bring Eq. (38), Eq. (39), and Eq. (41) into Eq. (48) to obtain the closed equations of ψ, θ, φ, w_1, w_2, w_3, which can be solved by numerical integration method.

The Ref. [22] and Ref. [23] established the cable dynamic model based on the accurate Cosserat elastic rod model, which is more suitable for the dynamic modeling of large deformation cables in engineering. The modeling meth-

ods in the two articles are essentially the same, so they relatively obtained a similar dynamic equations, but the equations of arc coordinates s in each dimension of the cable section principal axis coordinate system P-xyz due to the change of coordinates, and the expression of infinitesimal rotation basis vector generated by the section center in P-xyz are not derived. According to the force analysis of micro element, the Ref. [22] gives the correct unified equation for the partial differential calculation of force and moment, which provides a theoretical basis for the cable dynamics modeling. However, the third term of the moment partial differential equation of formula (19f) in Ref. [22] has an independent item angle θ. The independent term of θ and the lack of force and strain action components are also reflected in Ref. [23]. In this paper, the Eq. (48) proved that the angle θ should appear in the form of θ', that is in the form of the first derivative of the arc coordinate s. At the same time, the force and strain components are added in the Eq. (48).

5 Flexible Cable Simulation of Deployment Mechanism

The numerical method of adaptive step-size can be used to calculate the differential equations, so as to realize the rapid dynamic simulation of satellite mobile cable of assembly contact and collision. Set the physical parameters of cable as shown in Tab. 1.

The three-dimensional simulation model of the flexible cable of the deployment mechanism is established, as shown in Fig. 7. In the figure, the deployment mechanism and flexible cable model are simply simulated, the model includes a fixed part (fixed pair with the ground), a rotating part (rotating pair with the ground, the rotation center is the point O in the figure, and the rotation axis is z), and a flexible cable with physical properties as shown in Tab. 1. The connection between one end of the cable and the fixed part is a fixed connection, and the connection between the other end of the cable and the rotating part is a fixed connection, but it can follow the movement with the movement of the rotating part. Set the rotation speed of the rotating part around the z-axis to 1 (°)/s, ignore the effects of gravity, set the total simulation time is 90s, and the simulation step size is 1s.

Tab. 1 Simulation parameters of cable

Physical parameter	Symbol (Unit)	Value
Cable length	L (mm)	175
Cable diameter	D (mm)	10
Cable density	ρ (g·cm^{-3})	10
Section moment of inertia	$I_x I_y$ (mm^4)	490.874
Polar moment of inertia of section	I_z (mm^4)	981.748
Modulus of elasticity	E (GPa)	51.6
Shear modulus	G (GPa)	20.52
Bending stiffness	A, B (N·mm^2)	0.71×10^6
Torsional stiffness	C (N·mm^2)	0.54×10^6
Original bending and torsion	$\boldsymbol{\omega}^0$	(0 0 0)

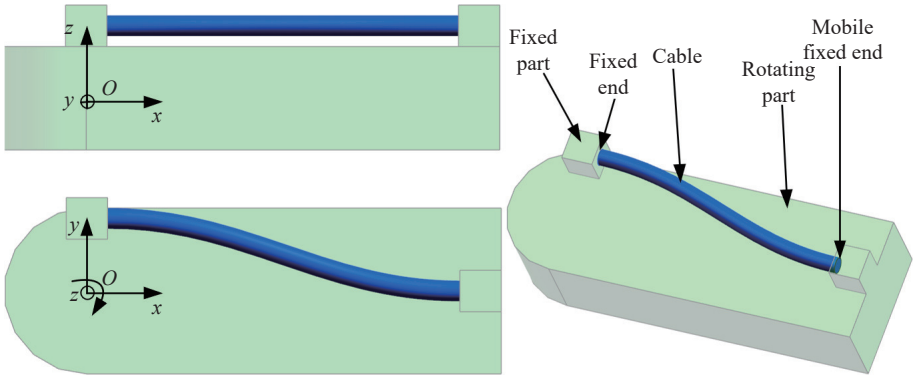

Fig. 7 Simulation model of deployment mechanism cable

The following movement of the flexible cable is obtained, as shown in Fig. 8. It can be seen that the fixed end of the flexible cable remains fixed with the earth during the movement of the rotating part; the mobile fixed end follows the movement of the rotating part, and achieves a good simulation effect. The cable changes from the initial relatively relaxed state to the tensioned state gradually, and there is a transitional bending and torsion phenomenon at the fixed end, which indicates that the cable will be subjected to large force and torque. It is necessary to increase the cable length to ensure that the cable remains relatively relaxed during the movement of rotating parts. It can be further demonstrated from the changes of forces and torques on the cable.

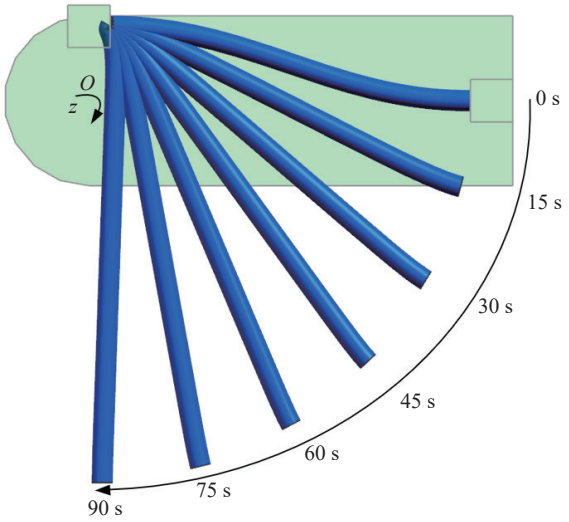

Fig. 8 Following motion of flexible cable of deployment mechanism

The force variation curves of the fixed end and the mobile fixed end of the cable are obtained, as shown in Fig. 9. It can be seen that the resultant force on the fixed end increases with the movement of the rotating part gradually, and the maximum value of the resultant force is 1319 N, in which the force in the x direction changes in a semi elliptical shape, while the force in the y direction changes in a quarter elliptical shape, which is related to the rotating part rotating around the z-axis, symmetrical in the x direction and asymmetric in the y direction, which is in line with the actual situation. The force of the resultant force on the fixed end of the cable in the z direction is almost zero, which is related to the non-gravity distribution force in the simulation environment, which is in line with the actual situation. The resultant force on the moving fixed end gradually increases with the movement of the rotating part, and the maximum value of the resultant force is 1319 N. Its component force in the x, y, z direction is almost the same as that of the fixed end resultant force in the x, y, z direction, and the direction is opposite. It can be seen that the resultant force of the two constraint ends on the cable is almost zero, which is related to the fact that the deployment mechanism is only provided with rotational motion.

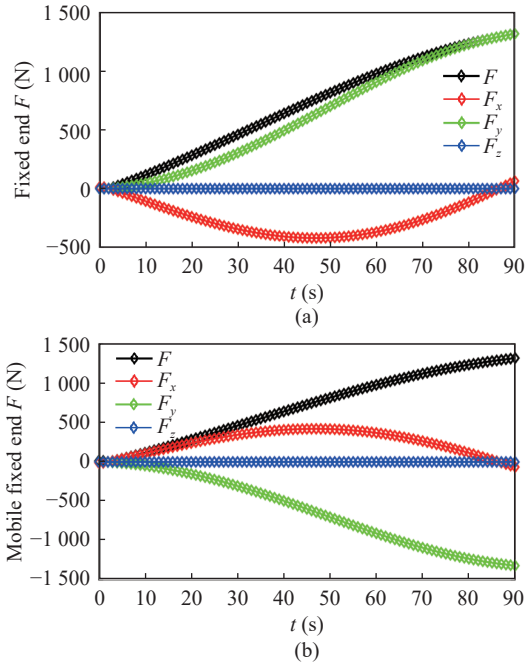

Fig. 9 Force change of fixed end and mobile fixed end of flexible cable: (a) force change of fixed end; (b) force change of mobile fixed end

The resultant force on the moving fixed end gradually increases with the movement of the rotating part, and the maximum value of the resultant force is 1319 N. Its component force in the x, y , z direction is almost the same as that of the fixed end resultant force in the x, y , z direc-

tion, and the direction is opposite. It can be seen that the resultant force of the two constraint ends on the cable is almost 0, which is related to the fact that the deployment mechanism is only provided with rotational motion.

The variation curve of the resultant moment of the fixed end and the mobile fixed end of the cable is obtained, as shown in Fig. 10. It can be seen that the resultant moment of the fixed end gradually increases with the movement of the rotating part, reaching the maximum value at about 78 s, with the maximum value of 5.25 N·m. the torque value decreases in 78 s –90 s. The moment at the mobile fixed end shows an approximate semi-elliptical variation trend, reaching the maximum value at about 35 s, and the maximum value is 0.69 N·m. Since the fixed end does not move with the rotating part, but produces large bending and torsional deformation with the movement of the rotating part, the torque value at the fixed end must be greater than that at the moving fixed end, which is in line with the actual situation.

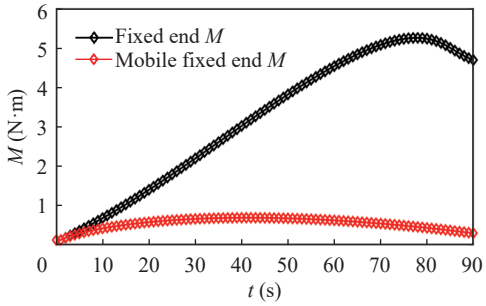

Fig. 10 Variation of the resultant moment of fixed end and mobile fixed end of flexible cable

6 Conclusions

This paper can be summarized as follows.

1) The Cosserat dynamic modeling of the mobile cable is established, and the existing mathematical model is improved. According to the Kardan angular coordinate transformation system, the matrix expression of the base vector after the center line transformation caused by shear deformation in the coordinate system without shear deformation is obtained, and six generalized coordinates in the cable dynamics are obtained. From this, the angular displacement vector, elastic strain equation, and velocity equation of the outgoing cable are derived, and the Cosserat dynamic model of the cable with arbitrary circular section is obtained according to the theorem of momentum and moment of momentum, which provides a theoretical basis for the dynamic calculation and simulation of the flexible cable.

2) The three-dimensional model and simulation of the flexible cable of the deployment mechanism are carried out, the trajectory of the flexible cable following the movement of the deployment mechanism is obtained, and the changes of the force and torque at the constraint end of the cable are obtained, which provides a reference for the dynamic simulation of the flexible cable.

3) The theory and simulation of cable dynamics and some simulation results are obtained. In the subsequent research, we can use the sensors of force, displacement, and transmitter devices, etc. to measure the parameters during the cable movement, and compare them with the simulation results. At the same time, the theoretical model in this paper can be compared with other dynamic models. For cables with the same physical properties, the calculation results obtained by different theories can be observed, so as to select a more appropriate theoretical model, and to improve the theory and simulation model further.

References:

[1] B. D. You, T. J. Zheng, J. Chen, and B. J. Yang, "Mechanics modeling of spacecraft cable considering spatial constraints, " *Journal of Vibration and Shock*, vol. 34, no. 16, pp. 8-13, 2015.

[2] W. T. Jin, J. H. Liu, J. S. Liu, C. T. Tang, and H. L. Lin, "Motional cable harness physical characteristic oriented modeling and kinetic simulation technology under smooth plane constraints, " *Journal of Mechanical Engineering*, vol. 52, no. 3, pp. 118-127, 2016.

[3] F. L. Wang, X. P. Guo, Z. N. Li, and L. K. Song, "Automatic extraction method for corresponding relationship among endpoint-to-location of cable wiring under coordinate system guidance, " *China Mechanical Engineering*, vol. 31, no. 14, pp. 1708-1716, 2020.

[4] J. H. Liu, T. Zhao, C. S. Wang, and C. T. Tang, "Motional cable harness physical characteristic oriented modeling and kinetic simulation technology in virtual environment, " *Journal of Mechanical Engineering*, vol. 47, no. 9, pp. 117-124, 2011.

[5] N. J. Lv, J. H. Liu, H. X. Xia, J. T. Ma, and X. D. Yang, "A review of techniques for modeling flexible cables, " *Computer-Aided Design*, vol. 122, pp. 102826, 2020.

[6] B. D. You, T. J. Zheng, J. Chen, B. J. Yang, and Y. Zhao, "Analyses and tests on mechanical properties of dragging flexible cables with large deformation, " *Journal of Mechanical Engineering*, vol. 51, no. 23, pp. 36-45, 2015.

[7] Y. Xue, D. W. Wong, and L. Q. Chen, "Methods of analytical mechanics for exact Cosserat elastic rod dynamics , " *Acta Physica Sinica*, vol. 62, no. 4, pp. 320-326, 2013.

[8] F. Kogelbauer and M. B. Rubin, "Free and forced whirling of a string with constant axial angular momentum using Cosserat point elements (CPE), " *International Journal of Solids and Structures*, vol. 152-153, pp. 196-206, 2018.

[9] M. Chadha and M. D. Todd, "A comprehensive kinematic model of single-manifold Cosserat beam structures with application to a finite strain measurement model for strain gauges, " *International Journal of Solids and Structures*, vol. 159, pp. 58-76, 2019.

[10] A. Papacharalampopoulos and S. Makris, "Twist modelling for assembly of wiring harnesses, " *Procedia CIRP*, vol. 97, pp. 71-75, 2021.

[11] H. Hu, Q. Tian and C. Liu, "Soft machines: Challenges to computational dynamics, " *Procedia IUTAM*, vol. 20, pp. 10-17, 2017.

[12] O. Dmitrochenko, "Finite elements using absolute nodal coordinates for large-deformation flexible multibody dynamics, " *Journal of Computational and Applied Mathematics*, vol. 215, no. 2, pp. 368-377, 2008.

[13] G. Fotland and B. Haugen, "Numerical integration algorithms and constraint formulations for an ALE-ANCF cable element, " *Mechanism and Machine Theory*, vol. 170, pp. 104659, 2022.

[14] A. R. Tusnin and O. A. Tusnina, "Numerical analysis of rod systems behavior after buckling, " *Procedia Engineering*, vol. 153, pp. 791-798, 2016.

[15] A. Arena, A. Pacitti, and W. Lacarbonara, "Nonlinear response of elastic cables with flexural-torsional stiffness, " *International Journal of Solids and Structures*, vol. 87, pp. 267-277, 2016.

[16] Y. Xue and D. W. Wong, "Gauss principle for a super-thin elastic rod dynamics, " *Acta Physica Sinica*, vol. 58, no. 1, pp. 34-39, 2009.

[17] T. Hermansson, R. Bohlin, J. S. Carlson, and R. Söderberg, "Automatic assembly path planning for wiring harness installations, " *Journal of Manufacturing Systems*, vol. 32, no. 3, pp. 417-422, 2013.

[18] N. J. Lv, J. H. Liu, X. Y. Ding, J. S. Liu, H. L. Lin, and J. T. Ma, "Physically based real-time interactive assembly simulation of cable harness, " *Journal of Manufacturing Systems*, vol. 43, pp. 385-399, 2017.

[19] J. A. Witz and Z. Tan, "On the flexural structural behaviour of flexible pipes, umbilicals and marine cables, " *Marine Structures*, vol. 5, no. 2, pp. 229-249, 1992.

[20] A. A. Sipos and P. L. Várkonyi, "A unified morphoelastic rod model with application to growth-induced coiling, waving, and skewing of plant roots, " *Journal of the Mechanics and Physics of Solids*, vol. 160, pp. 104789, 2022.

[21] W. Wu and X. Cao, "Mechanics model and its equation of wire rope based on elastic thin rod theory, " *International Journal of Solids and Structures*, vol. 102-103, pp. 21-29, 2016.

[22] Y. Z. Liu, "Cosserat modeling of thin-long curve beams with arbitrary shape in elastic medium, " *Engineering Mechanics*, vol. 31, no. 8, pp. 77-82, 2014.

[23] F. L. Wang, W. H. Liao, Y. Guo, and X. F. Wang, "Physical characteristics modeling and deformation simulation technology for flexible cable harness based on exact Cosserat model, " *Journal of Computer-Aided Design and Computer Graphics*, vol. 29, no. 7, pp. 1343-1355, 2017.

Ziquan Wang was born in Bozhou, Anhui Province, China in 1996. He received the B.S. degree in mechanical engineering and automation from Anhui University of Science and Technology, Huainan, Anhui, China, in 2013 and 2017, and received the M.S. degree in

mechanical designing and automation from Hefei University of Technology, Hefei, Anhui, China, in 2017 and 2020, respectively. From 2020 to present, he has been with the Satellite AIT Center, Shanghai Institute of Spacecraft Equipment, where he is currently a full production engineer. His main research directions are technological design of satellite engineering, mechanical and electronic engineering, embedded system development technology and hydraulic and pneumatic engineering.

Jinzhu Li is the director of Electric and Heating Installation Engineering Department of Shanghai Institute of Spacecraft Equipment and National Defense Basic Scientific Research Funding Project. His main research directions are technological design of satellite engineering, manufacturing of machinery, the complex systems of electromechanical, mechanical and electronic engineering and management engineering.

Weinan Chen is the director of Satellite Assembly Center of Shanghai Institute of Spacecraft Equipment and National Defense Basic Scientific Research Funding Project. His major research directions are technological design of satellite engineering, mechanical system dynamics, mechanical and electronic engineering, embedded system development technology, the complex systems of electromechanical and management engineering.

Xuefeng Gao is the director of Satellite Structure Products Division of Shanghai Institute of Spacecraft Equipment. His major research directions are technological design of satellite engineering, mechanical system dynamics, mechanical and electronic engineering, embedded system development technology and management engineering.

You Lü is the senior technician of Satellite Assembly Center of Shanghai Institute of Spacecraft Equipment, and mainly responsible for structure and electronic component assembly of satellite. His major research direction is technological design of satellite engineering.

Leijie Shen is the senior technician of Satellite Assembly Center of Shanghai Institute of Spacecraft Equipment, and mainly responsible for structure and electronic component assembly of satellite. His major research direction is technological design of satellite engineering.

Haojie Chen is the senior technician of Satellite Assembly Center of Shanghai Institute of Spacecraft Equipment, and mainly responsible for structure and electronic component assembly of satellite. His major research direction is technological design of satellite engineering.